nature catalysis

ARTICLES

https://doi.org/10.1038/s41929-017-0002-4

Electrophilic aromatic substitution over zeolites generates Wheland-type reaction intermediates

Abhishek Dutta Chowdhury[1], Klaartje Houben[2], Gareth T. Whiting[1], Sang-Ho Chung[1], Marc Baldus[2] and Bert M. Weckhuysen[1*]

The synthesis of many industrial bulk and fine chemicals frequently involves electrophilic aromatic substitution (S_EAr) reactions. The most widely practiced example of the S_EAr mechanism is the zeolite-catalysed ethylation of benzene, using ethylene as an alkylating agent. However, the current production route towards ethylbenzene is completely dependent on fossil resources, making the recent commercial successes in the zeolite-catalysed benzene ethylation process using bioethanol (instead of ethylene) very encouraging and noteworthy. Unfortunately, there is no information available on the reaction mechanism of this alternative synthesis route. Here, by employing a combination of advanced solid-state NMR spectroscopy and operando UV-Vis diffuse reflectance spectroscopy with on-line mass spectrometry, we have obtained detailed mechanistic insights into the bioethanol-mediated benzene ethylation process through the identification of active surface ethoxy species, surface-adsorbed zeolite–aromatic π-complexes, as well as the more controversial Wheland-type σ-complex. Moreover, we distinguish between rigid and mobile zeolite-trapped organic species, providing further evidence for distinctive host–guest chemistry during catalysis.

Electrophilic aromatic substitution (S_EAr) is one of the oldest and most important synthetic organic reactions to form carbon–carbon bonds. The reaction is proposed to involve the classical carbocationic σ-complex, which is better known as the Wheland intermediate, formed upon an attack by a π-electron-rich aromatic on an electrophile[1]. Since its discovery by Friedel and Crafts in 1877, S_EAr has been extensively utilized by the chemical industry to produce functionalized aromatic compounds[2,3]. For example, ethylbenzene is currently produced by the ethylation of benzene (EB) with ethylene using a zeolite catalyst (for example, the Mobil–Badger process, Universal Oil Products' (UOP) EBOne process, Mobil–Raytheon's EBMax process and UOP/CEPSA process), and is a very important chemical intermediate in the petrochemical industry for the production of styrene[3–7]. Currently, more than 99% of all ethylbenzene produced is used in the production of polystyrene-derived plastic materials[8]. Despite these industrial advancements, there are surprisingly no detailed studies discussing the S_EAr reaction mechanism of the zeolite-catalysed EB processes. The importance of mechanistic understanding of this industrially relevant reaction cannot be ignored, as such information is crucial to maximizing yields, reducing costs and minimizing waste in order to increase economic value[9]. Furthermore, this reaction is also of academic interest, as the underlying mechanistic principles of S_EAr are currently the subject of debate. According to a few recent studies, the classical Wheland intermediate is not always considered to be an obligatory intermediate during S_EAr[10–13]. Thus, the objectives of this work are to investigate the S_EAr mechanism at the solid/gas interface of a heterogeneous catalyst, and to resolve the ambiguity about the involvement of Wheland intermediates in zeolite-catalysed S_EAr reactions. To realize these ambitions, we have chosen the classical zeolite-catalysed ethylation of benzene, in which we use bio-ethanol instead of ethylene as the alkylating agent.

Traditionally, ethylbenzene is produced by homogeneous Friedel–Crafts-type Lewis acidic catalysts (for example, HF or $AlCl_3$), but disadvantages of this process include: corrosion, toxicity, waste disposal and halide impurities within aromatics[6–8]. In order to overcome these issues and achieve environmental tolerance and superior product selectivity through size control, zeolites (H-ZSM-5 and MCM-22) have been introduced by the petrochemical industry for the ethylene-mediated production of ethylbenzene, as they are heterogeneous catalysts that exhibit robust shape and size selectivity through regular micropores[6,14–16]. However, several drawbacks still exist, such as the application of external reaction pressure, contaminants in the olefin feed from fluid catalytic cracking units, faster catalyst deactivation (rapid coke formation due to oligomerization of olefins) and, importantly, complete dependency on fossil fuel feedstocks[7,8]. In order to reduce this dependency, the direct use of bioethanol (instead of ethylene) as an alkylating agent provides a more sustainable and economical option for the production of ethylbenzene[17]. Although, pioneering work on alcohol-mediated aromatic alkylation took place as early as 1966, efforts were discontinued due to low crude oil prices (compared with the price of alcohol)[18]. Nowadays, the situation is completely reversed due to the high price of fossil fuels and concerns about global climate change. Moreover, the current production scale and price of bioethanol from renewable biomass-derived resources (that is, ligno- and hemicelluloses) are also favourable enough to replace olefins within the industrial aromatic alkylation process[17]. Moreover, if aromatics can also be derived via depolymerization of lignocellulosic biomass materials (instead of fossil fuel) in future, then the complete EB process would be absolutely renewable[19]. Thus, the zeolite-catalysed EB process has recently captured renewed attention in both academia[16–26] and industry[16,27–30].

In this work, we establish a fundamental understanding on the reaction mechanism of the commercially relevant, zeolite-catalysed,

[1]Inorganic Chemistry and Catalysis Group, Debye Institute for Nanomaterials Science, Utrecht University, Utrecht, The Netherlands. [2]NMR Spectroscopy, Bijvoet Center for Biomolecular Research, Utrecht University, Utrecht, The Netherlands. *e-mail: B.M.Weckhuysen@uu.nl

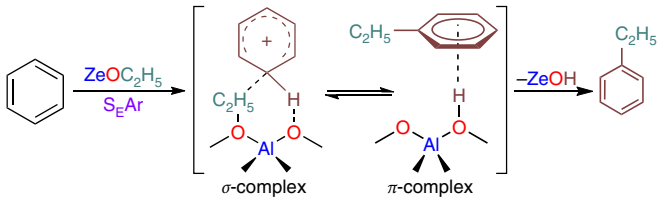

Fig. 1 | Schematic illustration of the zeolite-catalysed EB reaction. The EB reaction follows an S_EAr mechanism. This work provides experimental evidence in support of the formation of a surface ethoxy species ($ZeOC_2H_5$)-type active catalyst, carbocationic arenium ion/σ-complex (Wheland-type reaction intermediate) and neutral zeolite adsorbed aromatic π-complex.

bioethanol-mediated EB process; primarily through the identification of a surface ethoxy species (SES)-type active catalyst, as well as the Wheland-type carbocationic σ-complex and neutral zeolite adsorbed aromatic π-complex (Fig. 1). This has been made possible by operando UV-Vis diffuse reflectance spectroscopy (DRS) coupled with on-line mass spectrometry (MS), and corroborated with advanced multi-dimensional solid-state nuclear magnetic resonance (NMR) studies. As a result, new insights into the host–guest chemistry between the zeolite and aromatics, in terms of their surface mobility and reactivity, have also been obtained. The EB reaction was performed using millimetre-sized, alumina-bound H-ZSM-5 catalyst extrudates, using an equimolar ratio of benzene and ethanol as a reactant at 573 K. Details on the preparation and characterization of the alumina-bound H-ZSM-5 extrudate materials used in this study, can be found in the Supplementary Information (Supplementary Methods I and Supplementary Figure 1).

Results

Operando optical spectroscopy. In the first phase of our study, operando UV-Vis DRS coupled with on-line MS was used to identify and differentiate between neutral and carbocationic (including Wheland intermediates) organic species trapped within the zeolite material, as well as gas-phase products formed during the EB reaction over H-ZSM-5 extrudates at 573 K for 30 min (Supplementary Methods II). The results are summarized in Fig. 2 & Supplementary Fig. 2. The major spectral changes during the initial 10 min of reaction are illustrated in Fig. 2a, where the absorption bands at 295, 334, 415 and 596 nm increase in intensity with increasing time-on-stream (TOS). After ~7 min of reaction, the increase in intensity continues only for the 596 nm band (Fig. 2b,c and Supplementary Fig. 2a). The observed bands at ~295, 334 and 415 nm are attributed to neutral alkylated benzenes, carbenium ions with alkyl side chain carbocation and aromatic ring protonation, respectively, whereas the band at 596 nm presumably develops due to the existence of π-complexes between the zeolite and aromatic species (*vide infra* for NMR results)[31–39]. The on-line MS data reveal the existence of diethyl ether, lower olefins (ethylene and propylene) and ethylbenzene (Fig. 2d) along with traces of diethylbenzene and cumene (Supplementary Fig. 2c). Interestingly, the cross-section of the post-reacted extrudate develops a 'core–shell'-type bi-colouration (yellow and violet in the shell and core, respectively, Supplementary Fig. 2b).

In principle, alkylbenzenes could form two different types of carbocations/carbenium ions via only two routes: (i) Brønsted acid site

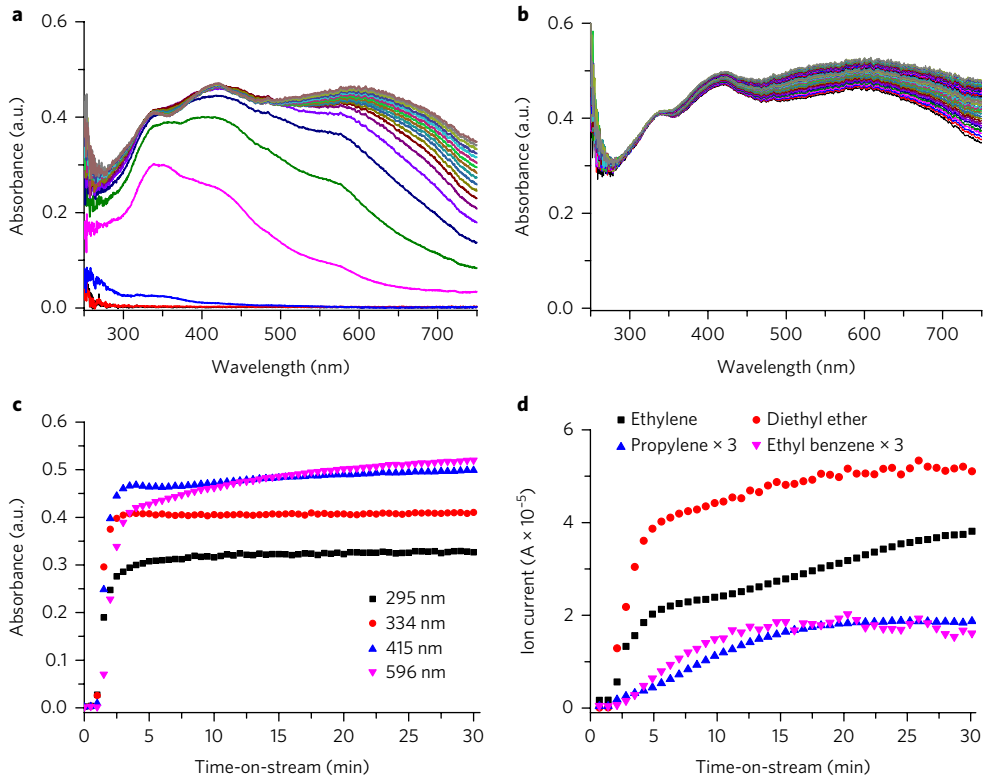

Fig. 2 | Operando UV-Vis DRS measurements during the EB reaction. a–d, Measurements conducted at 573 K over alumina-bound H-ZSM-5 extrudates for 0–10 min (**a**) and 10–30 min (**b**); time-resolved absorbance band changes (**c**) and mass spectral profiles (**d**) for ethylene, diethyl ether, propylene and ethylbenzene as a function of reaction time. Different colours in **a** and **b** indicate different measurement time during this time-monitored operando measurement. For the sake of clarity, the ion current of propylene and ethylbenzene is multiplied by three in **d**.

mediated formation of cyclohexadienyl (arenium) ions/σ-complex (that is, a Wheland-type intermediate) via protonation/alkylation of the aromatic ring (equation (1)) and (ii) Lewis acid side-promoted formation of alkylated carbenium ions via hydride abstraction from the alkyl chain of aromatics (equation (2))[33,37].

$$Ar{-}(CH_2)_n{-}CH_3 + H^+ \leftrightarrow Ar(H)^+{-}(CH_2)_n{-}CH_3 \quad (1)$$

$$Ar{-}(CH_2)_n{-}CH_3 \leftrightarrow Ar{-}(CH_2)_n{-}CH_{2^+} + H^- \quad (2)$$

The existence of Wheland intermediates during the EB reaction over the zeolite was confirmed by a series of experiments using UV-Vis DRS, upon electronic variation of both electrophile (ZeOX, X = H and C_2H_5) and nucleophile (C_6H_5R, R = H, C_2H_5 and OCH_3) (Fig. 3, Supplementary Figs. 3–6 and Supplementary Methods II)[31–38]. Figure 3a–d reflects a redshift of the absorption maxima of a σ-complex (Wheland species), either upon ethylation of the zeolite or in the presence of an electron-donating group attached to the aromatic ring. Moreover, both the ethylation of ethylbenzene and the protonation of 1,4-diethylbenzene were observed to have an identical Wheland-type reaction intermediate, which was identified and absorbs light at ~421 nm (highlighted in green, Fig. 3e). These UV-Vis DRS experiments unequivocally support the existence of a carbocationic σ-complex (that is, Wheland intermediate) during the zeolite-catalysed alkylation of aromatics, which is known to follow

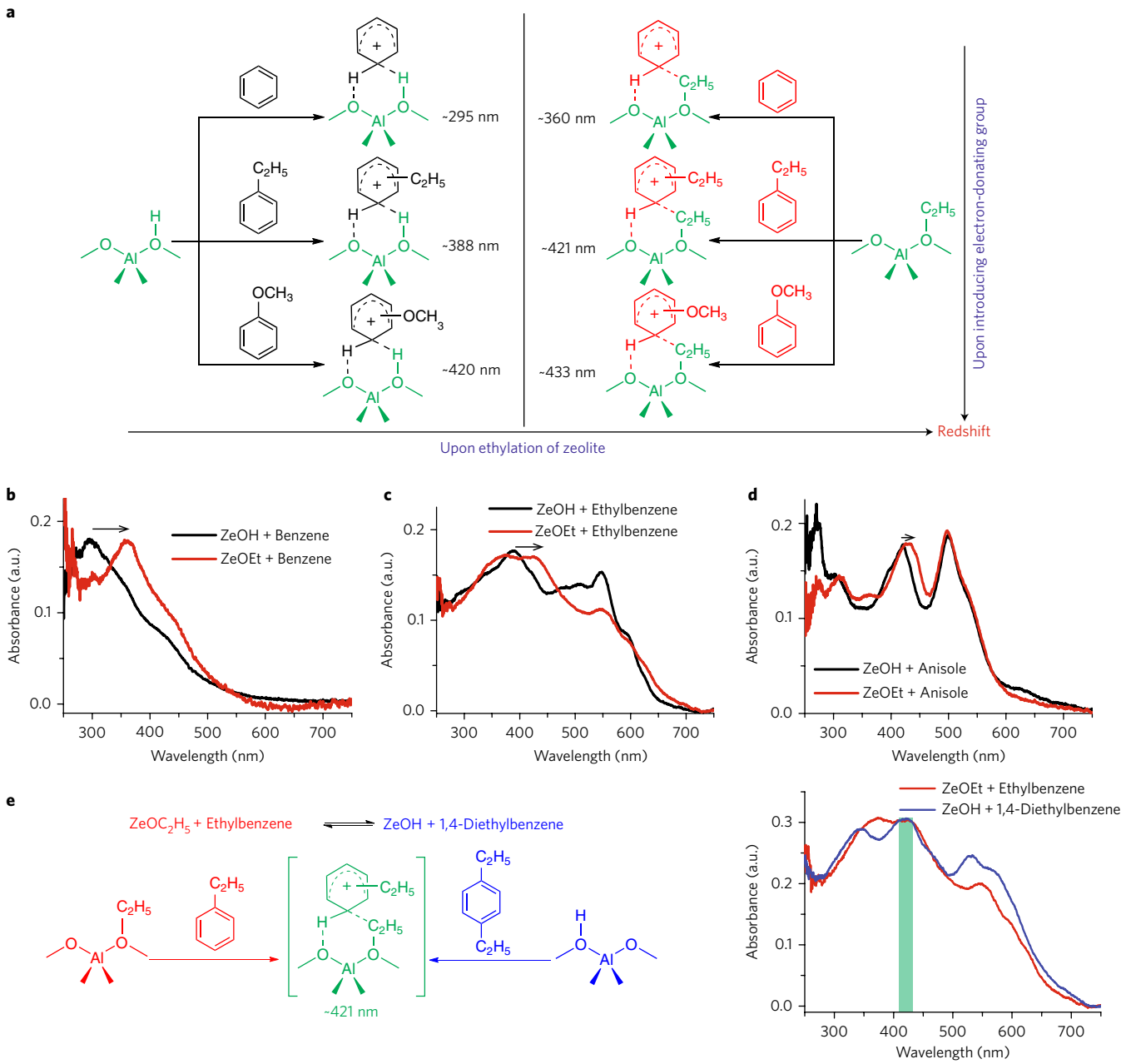

Fig. 3 | The electronic effect on the formation of a Wheland-type reaction intermediate during the zeolite-catalysed ethylation of aromatics. **a**, Schematic illustration of measurements conducted upon altering both electrophile (ZeOX, X = H and C_2H_5) and nucleophile (C_6H_5R, R = H, C_2H_5 and OCH_3). **b**–**d**, Operando UV-Vis DRS spectroscopy measured at 393 K on an alumina-bound H-ZSM-5 (black) and C_2H_5-ZSM-5 (red) extrudate after the chemisorption of benzene (**b**), ethylbenzene (**c**) and anisole (**d**). **e**, Operando UV-Vis DRS spectroscopy measured at 393 K on an alumina-bound H-ZSM-5 extrudate after adsorption of 1,4-diethylbenzene (blue) and on an alumina-bound C_2H_5-ZSM-5 extrudate after adsorption of ethylbenzene (red).

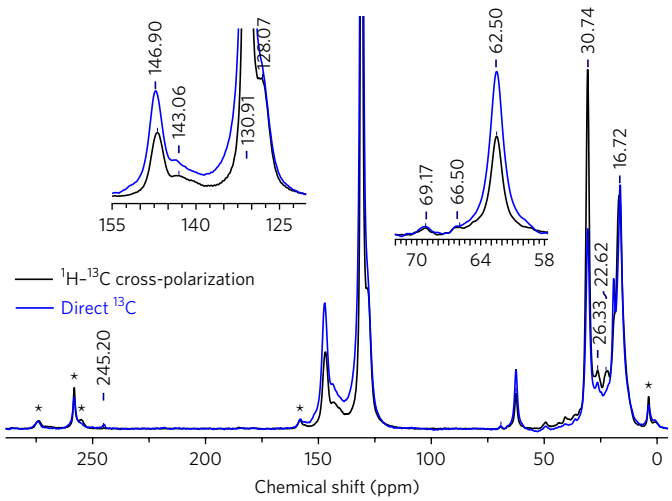

Fig. 4 | 1D ^{13}C solid-state NMR spectra of zeolite trapped products after EB reaction. The spectra are of trapped products obtained after the EB reaction over alumina-bound H-ZSM-5 extrudates at 573 K for 30 min (* = spinning sideband), with ^{13}C direct excitation in blue and ^{1}H–^{13}C cross-polarization in black.

an S_EAr mechanism. Furthermore, we have also shown the distinctive spectral influence of zeolite acid sites (both Brønsted and Lewis) and the binder (alumina) during the EB reaction (Supplementary Methods II including Supplementary Figs. 4–6).

Solid-state NMR spectroscopy. In the next phase of our study, we performed advanced magic angle spinning (MAS) solid-state NMR on alumina-bound H-ZSM-5 extrudates after the EB reaction was performed for 30 min at 573 K, using fully ^{13}C-enriched reactants. In the 1D ^{13}C-spectra (Fig. 4) of the EB-reacted catalyst, the following three features were observed: (i) 16–31 ppm aliphatic and methyl groups, (ii) 58–70 ppm ethoxy groups, and (iii) 125–150 ppm aromatic groups (Supplementary Methods III–IV and Supplementary Table 1). The strongest aromatic signal at ~131 ppm contains a contribution mostly from the unreacted zeolite-trapped benzene molecules, while the peaks at ~62, 66 and 69 ppm are due to surface adsorbed ethanol, diethyl ether and SES, respectively (Supplementary Figs. 9,10)[40].

Using isotope-enriched reactants not only significantly increased NMR sensitivity, but also allowed multi-dimensional solid-state NMR correlation experiments, which provide detailed insight into molecular structures. Moreover, we adapted different solid-state NMR magnetization transfer techniques previously developed for spectral separation of biomolecules on the basis of their mobility to distinguish between mobile species and molecules associated with or trapped in extrudates (Figs. 5,6 and Supplementary Figs. 7–12)[41,42]. Such species can be spectrally separated in NMR by using magnetization transfer schemes that invoke through-bond (scalar interactions such as in INEPT[43]) or through-space (dipolar transfer such as in cross-polarization[44]). Using the latter dipolar mechanism, molecules that exhibit no (such as physisorbed in or on the catalyst material) or limited (such as in the case of a molecule trapped within the zeolite structures) motion will predominantly appear in those spectra under our experimental conditions. On the other hand, in through-bond mediated schemes we will mostly observe molecules that exhibit fast overall tumbling or contain locally mobile groups such as seen in methyl groups that display fast rotation around the C–C axis. Using direct excitation such as shown in Fig. 4, all chemical species, including those that exhibit intermediate dynamics, can be observed.

In 2D and 3D solid-state NMR experiments probing mobile molecules (Fig. 5), we readily identified the unreacted reactants, ethanol (signals indicated by triangles) and benzene (white circles), as well as signals compatible with the products diethylbenzene (white squares), cumene (black diamonds) and tetramethylbenzene (black stars). For example, the methyl group at 24.7 (^{13}C) and 0.97 (^{1}H) ppm (black diamond Fig. 5b) shows cross-peaks with ^{1}H nuclei resonating at 2.65 and 7.02 ppm in the 3D ^{1}H–^{13}C–^{1}H experiment with 100 ms ^{1}H–^{1}H mixing (strip VI in Fig. 5c). Together with the corresponding ^{13}C frequencies (strips VII and VIII Fig. 5c: 36.4 and 127.8 ppm, respectively) and the intensity ratios of the two aliphatic resonances in the C–H spectrum (black diamonds Fig. 5b), we could readily assign this spin-system as isopropyl benzene (cumene).

Interestingly, for tetramethylbenzene, as well as for benzene, a cross-peak with a non-^{13}C-labelled molecular unit, that is, most probably, a Brønsted acidic OH group of the zeolite and/or the OH of ethanol (blue line and circles in Fig. 5c), was observed. Proximity to the zeolite was further confirmed by ^{13}C-filtered NMR spectra (Supplementary Fig. 12), where additional non-^{13}C-bound ^{1}H signals were identified. These cross-peaks indicate that, although highly mobile, such aromatic moieties are in close contact with the zeolite surface. It should be noted that the origin of these ^{1}H–^{1}H cross-peaks could either be the result of a direct dipolar interaction between two ^{1}Hs or due to chemical exchange. The methyl signal (indicated with a cross in Fig. 5b) was tentatively assigned to dimethylbenzene, based on the virtually identical spin-system and partial overlap with signals from tetramethylbenzene. Remaining aliphatic signals in the ^{1}H–^{13}C correlation spectrum (grey circles in Fig. 5b) could not be connected to other signals in these spectra (Supplementary Table 2). We speculate that these signals belong to mobile aliphatic substituents of rigid molecules, such as seen in methyl groups that display fast rotation around the C–C axis.

In the solid-state NMR spectra probing rigid molecules (Fig. 6), reactants (ethanol (**1a**) and benzene), the ethylating agent (SES) and products (ethylbenzene (**1b**) and diethylbenzene (**1c**)) were clearly distinguishable. For example, the typical methyl resonance at 17.3 ppm (Fig. 6, green spectrum) shows cross-peaks with three other ^{13}C resonances in the ^{13}C–^{13}C correlation spectra: one aliphatic resonance at 31.0 ppm and two aromatic resonances at 128.1 and 147.2 ppm (Fig. 6, red spectra, denoted by **1b**). This is a typical signature of an ethylated benzene ring. An identical spin-system with just slightly different chemical shifts could also be identified at 16.6, 30.6, 130.6 and 147.2 ppm (Figs. 1c,6). We therefore assigned these two spin-systems to mono- (**1b**) and diethylbenzene (**1c**). The existence of these rigid/immobilized π-complexes of zeolite-adsorbed aromatics (**1b**, **1c**) is consistent with the observations from optical spectroscopy (Supplementary Fig. 6). The chemical shifts of surface adsorbed ethanol were all shifted downfield, when compared with mobile ethanol (Supplementary Table 1), indicating that the local physical environment altered the electronic state of the immobilized ethanol. Such a deshielding effect could be related to the removal of local electron density through a hydrogen-bond network with the zeolite surface (**1a**) or due to the higher electron negativity of the zeolite surface. In case of hydrogen bonding with the zeolite, the shift could result from a lowered LUMO energy level and a corresponding reduced energy gap between frontier orbitals[45]. These chemical shifts were further confirmed by a separate control solid-state NMR experiment, recorded on alumina-bound H-ZSM-5 extrudates, impregnated with ^{13}C-ethanol (Supplementary Fig. 7). 2D solid-state NMR cross-peaks for both SES and surface-adsorbed ethanol (**1a**), appeared to be more intense in the direct excitation spectrum at lower temperature (Fig. 6, purple spectrum), highlighting the presence of their intermediate dynamics. For benzene, a similar chemical shift difference between the mobile molecule and its zeolite adduct is also observed, but the effect is less pronounced (Supplementary Table 1 and Supplementary Fig. 8).

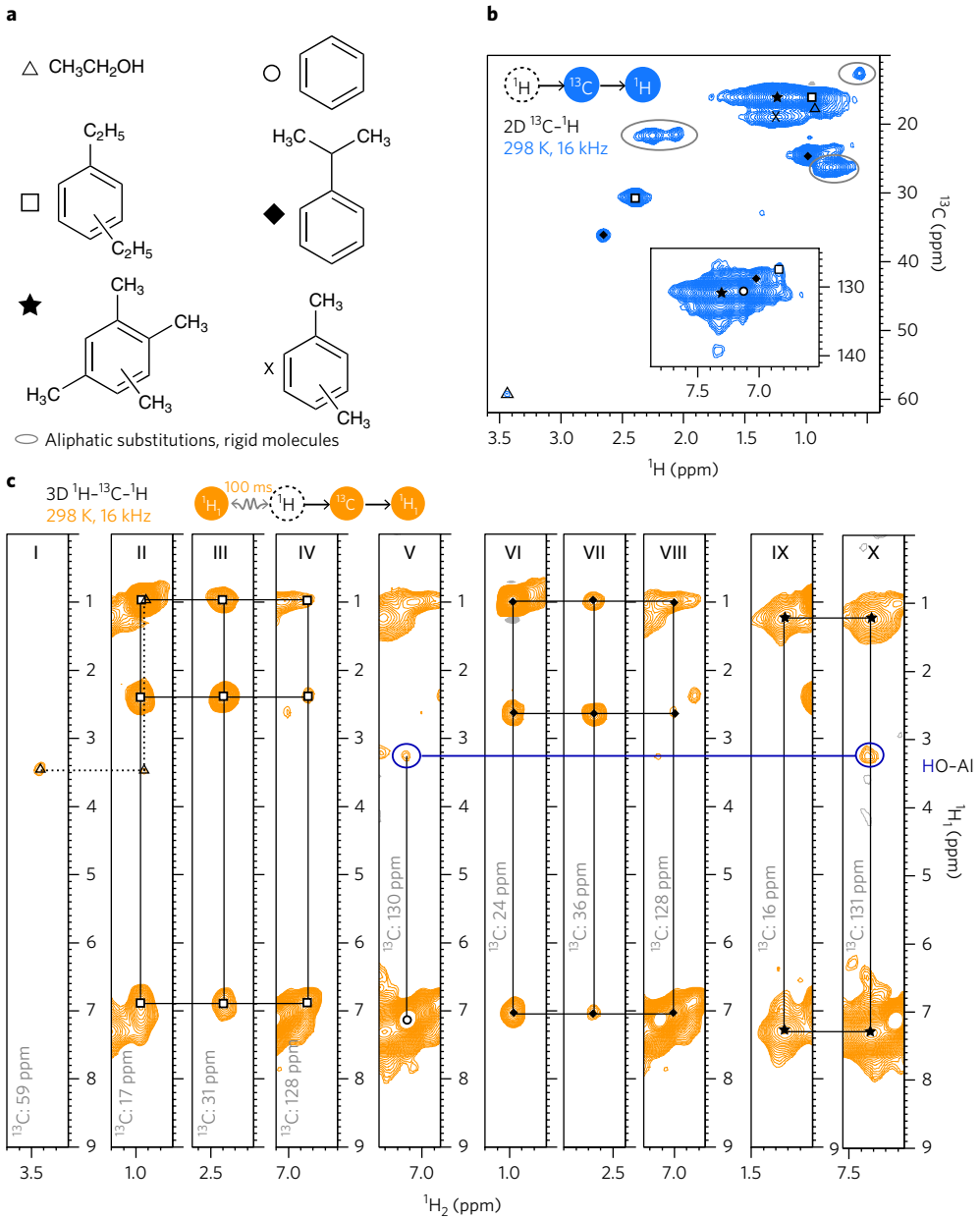

Fig. 5 | ^{13}C mobile molecules in *J*-coupling-based MAS solid-state NMR spectra. Spectra of trapped products obtained after the EB reaction over alumina bound H-ZSM-5 extrudates at 573 K for 30 min. **a**, Identified molecules. **b**, ^{13}C–^{1}H correlation spectrum. **c**, ^{1}H–^{1}H strips at different ^{13}C frequencies from a 3D ^{1}H–^{13}C–^{1}H correlation spectrum, with longitudinal ^{1}H–^{1}H mixing[50]. Vertical and horizontal lines indicate intramolecular polarization transfer or would be consistent with intermolecular transfer to an HO–Al site (blue line).

Moreover, a very weak signal at 245 ppm, solely observed in the 1D direct excitation experiment (Fig. 4), as well as low-intensity cross-peaks from a signal at 25.5 ppm to both 245 ppm and 157 ppm in the ^{13}C–^{13}C correlation spectra (Supplementary Fig. 9), are indicative of the formation of such alkylated carbenium species/σ-complex. Even though these correlations are consistent with the existence of a carbocationic fragment, its complete molecular structure could not be derived due to the absence of additional correlations. Such partial elucidation (weak/absent NMR signals) of the σ-complex (Wheland-type intermediate) could be attributed to the lower stability compared to its π-complex analogue (possibly due to loss of aromaticity, *vide infra* for mechanistic details) and putative line-broadening of certain signals caused by chemical exchange. It is worth mentioning that in situ UV-Vis spectroscopy is far more sensitive in the detection of any carbocation than solid-state NMR. In general, the detection of zeolite-surface-adsorbed π-complexes of ethylbenzene (**1b**) and diethylbenzene (**1c**) by ex situ solid-state NMR is consistent with the formation of a σ-complex (Wheland-type) intermediate during the EB reaction, and is also consistent with in situ/operando optical spectroscopy and the typical S_EAr mechanism[13]. Additional minor cross-peaks in the ^{13}C–^{13}C correlation spectra could not be assigned (Supplementary Figs. 9–11 and Supplementary Table 2).

Catalytic cycle and other mechanistic aspects. Based on the above-described results, a catalytic pathway for the EB reaction is proposed in Fig. 7. Firstly, ethanol is trapped on the zeolite via a hydrogen-bonded interaction with a Brønsted acid site (denoted as ZeOH in Fig. 7). Then, the surface-adsorbed ethanolic species (**1a**) either converts directly to SES (ethylation of ZeOH), or eliminates

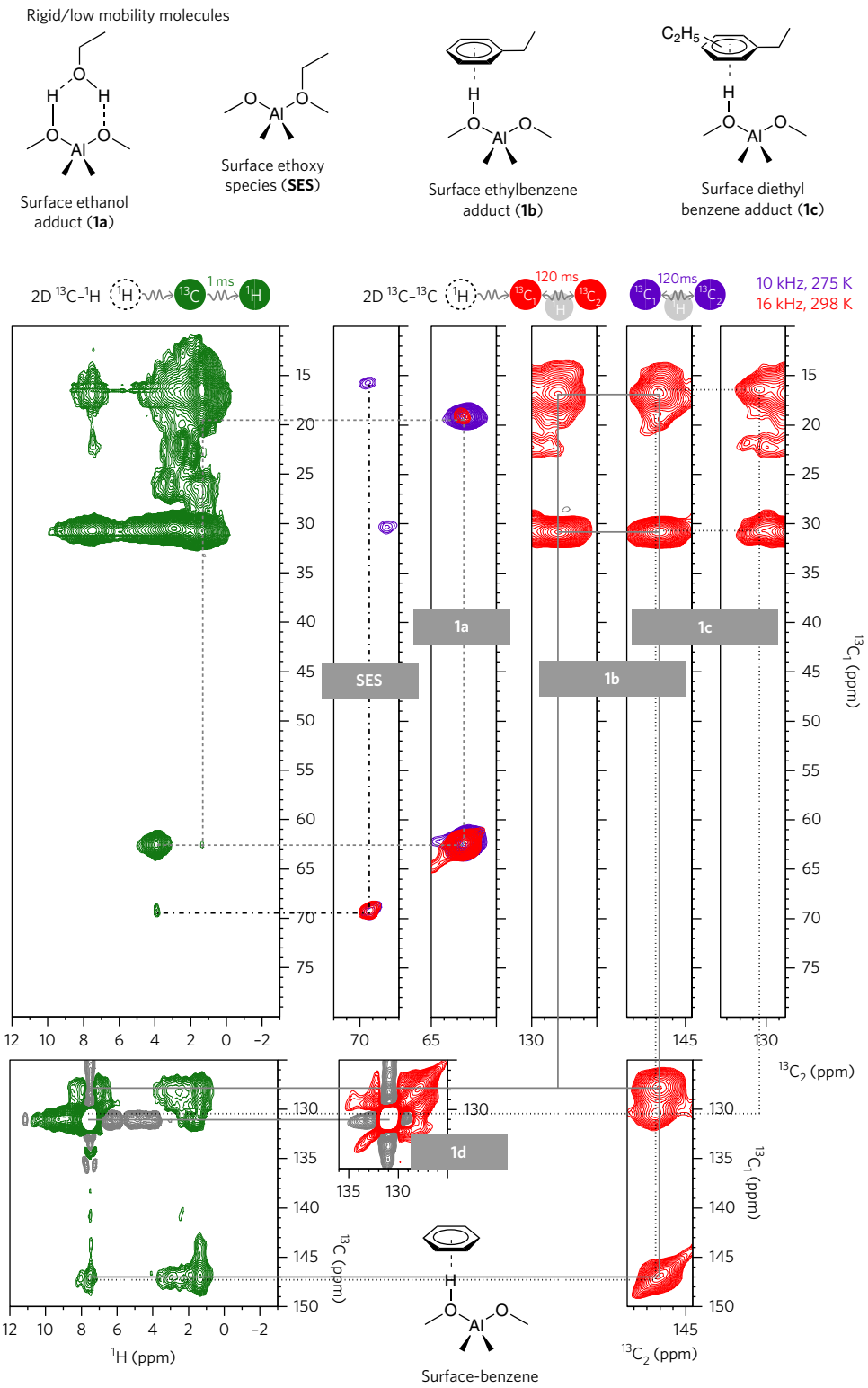

Fig. 6 | MAS solid-state NMR correlations of rigid zeolite trapped molecules. Spectra obtained after the EB reaction over alumina-bound H-ZSM-5 extrudates at 573 K for 30 min. For the ^{13}C–^{1}H correlation spectrum (green) dipolar cross-polarization was used to polarize the carbons. In the ^{13}C–^{13}C correlation spectra, the carbons were polarized either through cross-polarization (red) or direct excitation (purple) and ^{13}C–^{13}C mixing was achieved through proton-driven spin-diffusion using phase-alternated recoupling irradiation schemes (PARIS)[51].

ethylene (dehydration of ethanol). This ethanol dehydration process does not involve the formation of any carbocation, as was computationally and spectroscopically verified by Kim et al.[46] and Kondo et al.[47], respectively. However, ethylene could react further with ZeOH to form an SES (cycle A, Fig. 7). Next, our NMR study reveals the existence of zeolite-surface-adsorbed benzene molecules. Therefore, the high electron density at the benzene ring could tune its reactivity as a Lewis or a Brønsted–Lowry base, in order to interact

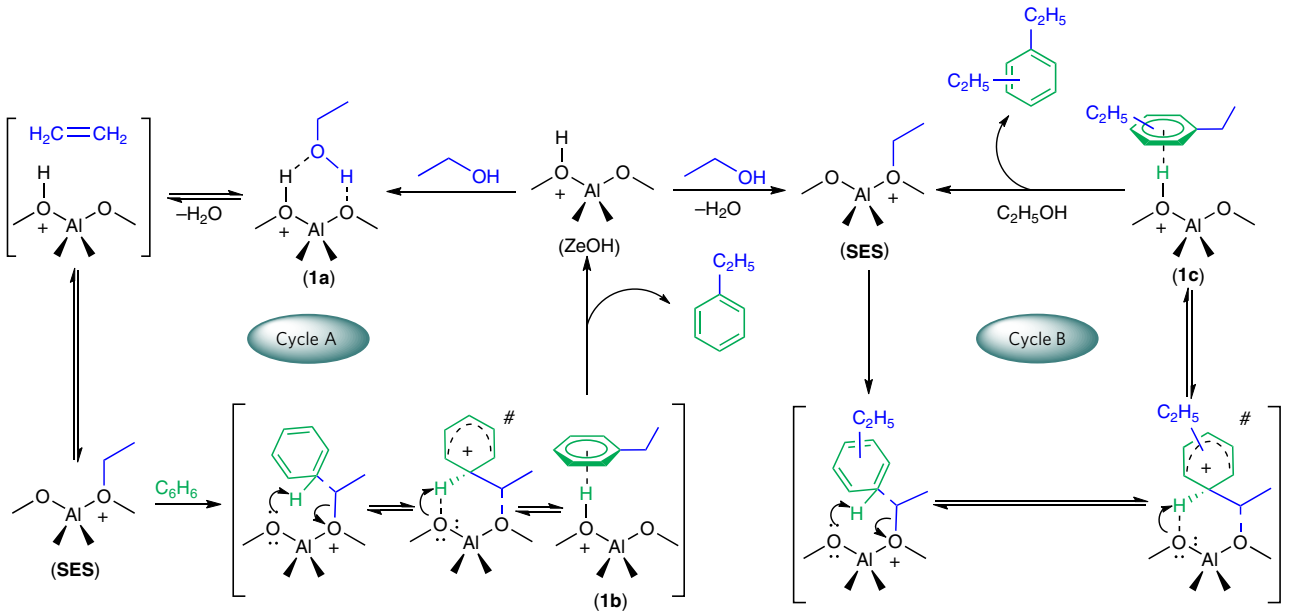

Fig. 7 | Proposed catalytic cycle of the zeolite catalysed EB reaction. All these reaction products and intermediates have been experimentally verified in this work (#, Wheland species).

with the Lewis or Brønsted acid site of the zeolite, respectively[48]. As a consequence, the interaction between an electrophilic SES and a nucleophilic π-system of the benzene ring is inevitable within a zeolite framework. In accordance with the typical S_EAr mechanism, benzene then attacks SES to form a σ-complex (Wheland-type) intermediate (denoted by # in cycle A, Fig. 7)[13]. Since this step involves temporary disruption of the aromatic π-system, it is considered as the rate-determining step in the S_EAr mechanism. This Wheland intermediate is, of course, less stable than the starting materials or the product, but it is a reasonably stable carbocation due to delocalization around its six-membered ring. Moreover, such Wheland intermediates might restrict themselves in the vicinity of a negatively charged Al defect and/or Al site (Al–O–Si) of the zeolite framework[49].

Once the Wheland complex is formed, the final step of the reaction starts immediately in order to restore aromaticity. It involves a transfer of the protonic hydrogen of the benzene to the zeolite, which leads to the formation of a zeolite-surface-adsorbed π-complex of ethylbenzene (**1b** in Fig. 7). Thus, solid-state NMR primarily detects the neutral species, after the loss of a proton from the Wheland intermediate/σ-complex, whereas the latter was identified predominantly by UV-Vis DRS. Next, the product, ethylbenzene, detaches itself from the surface and regenerates the zeolite (Al–OH–Si) during the course of the reaction (cycle A, Fig. 7). Finally, the surface diethylbenzene species (**1c**) is formed from an analogous Wheland-type species (denoted by # in cycle B, Fig. 7), which was generated upon the interaction between ethylbenzene and SES.

The presence of cumene indirectly justifies that olefins are indeed responsible for the formation of surface alkoxy species during the EB reaction. As illustrated in Supplementary Fig. 13, the surface propoxy species (SPS) is formed due to the interaction between zeolite and propylene, which later undergoes the S_EAr pathway with benzene to form cumene. From a different perspective, benzene is efficiently acting as a trapping agent to various electrophiles (either olefin or SES) during the EB reaction, in order to prevent the ethanol-derived homologation/chain growth reaction to form higher aromatics, which is an established phenomenon during zeolite catalysed alcohol conversion processes[26,34]. The other zeolite-trapped minor products, like xylene or tetramethylbenzene, are formed as a result of isomerization of ethylbenzene and diethylbenzene, respectively, under the experimental conditions of the EB reaction (Supplementary Fig. 14)[9].

Conclusions

In order to address the mechanistic aspects of the S_EAr reaction mechanism at the solid/gas interface, our complementary multimodal spectroscopic approach provides evidence in support of the formation of surface ethoxy species (the ethylating agent), Wheland intermediates (σ-complex between electrophilic SES and nucleophilic benzene), surface-ethylbenzene adducts (π-complex after the formation of the C–C bond) and deactivated products (diethylbenzene, cumeme, xylene and tetramethylbenzene) during the EB reaction using industrial-grade alumina-bound zeolite H-ZSM-5 extrudates. Thus, the existence of Wheland-type reaction intermediates could be confirmed in the mechanism of the zeolite catalysed S_EAr mechanism. Moreover, two different types of zeolite-trapped organic species were identified (mobile and rigid). Knowledge of such mobility-dependent features of surface-trapped organics in heterogeneous catalysis will not only be useful for the development of superior and/or upgraded catalyst materials for the EB reaction (via designing zeolite catalysts to mimic transition states of reactions)[9], but also contribute to the basic understanding of zeolite-catalysed hydrocarbon conversion chemistry.

Methods

The preparation and characterization of alumina-bound H-ZSM-5 extrudates along with experimental details of operando catalytic and control experiments are given in the Supplementary Methods. H-ZSM-5, ^{12}C-benzene/ethanol and ^{13}C-benzene/ethanol were purchased from ACS materials, Sigma Aldrich and Cambridge Isotope Laboratories, respectively. Catapal D (alumina) was received from Sasol. Zeolite extrudates were prepared using a Caleva Mini-Screw Extruder. A Caleva Mixer Torque Rheometer was used to optimize the solid-to-liquid ratio. Extrudates were finally calcined in a convection oven at 873 K for 6 h (rate: 5 K min^{-1}) under flowing air. Mercury intrusion was measured in a Micromeritics Autopore IV 9500 instrument. A contact angle of 130° for mercury intrusion and a pressure equilibration of 10 s were applied. Fourier transform infrared spectra in transmission mode were recorded on a PerkinElmer 2000 instrument. SEM was performed using FEI Helios Nanolab G3 instrument. Ar physisorption was performed with an automated gas sorption system

Micromeritics TriStar 3000. All catalytic reactions were performed using a Linkam cell (THMS600) equipped with a temperature controller (Linkam TMS94). The UV-Vis DRS measurements were performed with a CRAIC 20/30 PV UV-Vis-NIR micro-spectrophotometer using a 15× objective. A 75 W xenon lamp was used for illumination. The on-line gas phase product analyses were performed by a Pfeiffer OmniStar GSD 320 O3 (1–300 a.m.u.) mass spectrometer. The mass spectrometry database from the National Institute of Standards and Technology was consulted for assignment purposes. Optical images were taken using an Olympus BX41 M microscope. For solid-state NMR measurements, extrudates were crushed and transferred to a 3.2 mm rotor for MAS solid-state NMR experiments. All experiments were performed on a Bruker 500 MHz wide-bore magnet with an AVANCE-III console and equipped with a 3.2 mm HXY probe in double channel ^{1}H, ^{13}C mode. All experiments were performed at room temperature (298 K) and an MAS frequency of 16 kHz, or 275 K and 10 kHz. Note that effective sample temperatures can be 5–10 degrees higher due to frictional heating. Referencing of ^{1}H and ^{13}C chemical shifts was done externally to adamantane.

Data availability. The data that support the plots within this paper and other findings of this study are available from the corresponding author upon reasonable request.

Received: 20 May 2017; Accepted: 11 October 2017;
Published online: 20 November 2017

References

1. Allemann, O., Duttwyler, S., Romanato, P., Baldridge, K. K. & Siegel, J. S. Proton-catalyzed, silane-fueled Friedel-Crafts coupling of fluoroarenes. *Science* **332**, 574–577 (2011).
2. Friedel, C. & Crafts, J. M. *Sur une nouvelle méthode générale de synthèse d'hydrocarbures, d'acétones, etc. Compt. Rendus* **84**, 1392–1395 (1877).
3. Vogt, E. T. C., Whiting, G. T., Dutta Chowdhury, A. & Weckhuysen, B. M. Zeolites and zeotypes for oil and gas conversion. *Adv. Catal.* **58**, 143–314 (2015).
4. Busca, G. Acid catalysts in industrial hydrocarbon chemistry. *Chem. Rev.* **107**, 5366–5410 (2007).
5. Čejka, J. & Wichterlová, B. Acid-catalyzed synthesis of mono- and dialkyl benzenes over zeolites: active sites, zeolite topology, and reaction mechanisms. *Catal. Rev. Sci. Eng.* **44**, 375–421 (2002).
6. Perego, C. & Ingallina, P. Recent advances in the industrial alkylation of aromatics: new catalysts and new processes. *Catal. Today* **73**, 3–22 (2002).
7. Al-Khattaf, S., Ali, M. A. & Čejka, J. in *Zeolites and Catalysis: Synthesis, Reactions and Applications* (eds Čejka, J., Corma, A. & Zones, S. I.) Ch. 20, 623–648 (Wiley-VCH, Weinheim, 2010).
8. Al-khattaf, S. et al. Recent advances in reactions of alkylbenzenes over novel zeolites: the effects of zeolite structure and morphology. *Catal. Rev. Sci. Eng.* **56**, 333–402 (2014).
9. Gallego, E. M. et al. 'Ab initio' synthesis of zeolites for preestablished catalytic reactions. *Science* **27**, 1051–1054 (2017).
10. Galabov, B. et al. Arenium ions are not obligatory intermediates in electrophilic aromatic substitution. *Proc. Natl Acad. Sci. USA* **111**, 10067–10072 (2014).
11. Koleva, G., Galabov, B., Kong, J., Schaefer, H. F. & von R. Schleyer, P. Electrophilic aromatic sulfonation with SO_3: concerted or classic S_EAr mechanism? *J. Am. Chem. Soc.* **133**, 19094–19101 (2011).
12. Galabov, B., Nalbantova, D., Schleyer, P., von, R. & Schaefer, H. F. Electrophilic aromatic substitution: new insights into an old class of reactions. *Acc. Chem. Res.* **49**, 1191–1199 (2016).
13. Olah, G. A. Aromatic substitution. XXVIII. Mechanism of electrophilic aromatic substitutions. *Acc. Chem. Res.* **4**, 240–248 (1971).
14. Chen, N. Y. & Garwood, W. E. Industrial application of shape-selective catalysis. *Catal. Rev. Sci. Eng.* **28**, 185–264 (1986).
15. Kaeding, W. W., Barile, G. C. & Wu, M. M. Mobil zeolite catalysts for monomers. *Catal. Rev. Sci. Eng.* **26**, 597–612 (1984).
16. Yang, W., Wang, Z., Sun, H. & Zhang, B. Advances in development and industrial applications of ethylbenzene processes. *Chin. J. Catal.* **37**, 16–26 (2016).
17. Sun, J. & Wang, Y. Recent advances in catalytic conversion of ethanol to chemicals. *ACS Catal.* **4**, 1078–1090 (2014).
18. Venuto, P. B., Hamilton, L. A. & Landis, P. S. Organic reactions catalyzed by crystalline aluminosilicates. *J. Catal.* **493**, 484–493 (1966).
19. Rinaldi, R. et al. Paving the way for lignin valorisation: recent advances in bioengineering, biorefining and catalysis. *Angew. Chem. Int. Ed.* **55**, 8164–8215 (2016).
20. Corma, A., Llopis, F. J., Martínez, C., Sastre, G. & Valencia, S. The benefit of multipore zeolites: catalytic behaviour of zeolites with intersecting channels of different sizes for alkylation reactions. *J. Catal.* **268**, 9–17 (2009).
21. Odedairo, T. & Al-khattaf, S. Ethylation of benzene: effect of zeolite acidity and structure. *Appl. Catal. A Gen.* **385**, 31–45 (2010).
22. Odedairo, T. & Al-khattaf, S. Comparative study of zeolite catalyzed alkylation of benzene with alcohols of different chain length: H-ZSM-5 versus mordenite. *Catal. Today* **204**, 73–84 (2013).
23. Ding, W., Cui, Y., Li, J. & Fang, W. Promoting effect of dual modification of H-ZSM-5 catalyst by alkali treating and Mg doping on catalytic performances for alkylation of benzene with ethanol to ethylbenzene. *RSC Adv.* **4**, 50123–50129 (2014).
24. Christensen, C. H., Johannsen, K., Schmidt, I. & Christensen, C. H. Catalytic benzene alkylation over mesoporous zeolite single crystals: improving activity and selectivity with a new family of porous materials. *J. Am. Chem. Soc.* **125**, 13370–13371 (2003).
25. Chandawar, K. H., Kulkarni, S. B. & Ratnasamy, P. Alkylation of benzene with ethanol over ZSM-5 zeolites. *Appl. Catal.* **4**, 287–295 (1982).
26. Fort, A. W. & Davis, B. H. Carbon-14 rearrangement in the alkylation of benzene with ethanol over ZSM-5 catalyst. *J. Catal.* **96**, 357–362 (1985).
27. Ghosh, A. K., Shafiei, M., Castelan, M., Harvey, P. & Kulkarni, N. Pretreatment of a phosphorous modified zeolite catalyst for an aromatic alkylation process. US patent 8115041 B2 (2012).
28. Chu, Y. F., Marler, D. O. & McWilliams, J. P. Alkylation of aromatics. US patent 005157185A (1992).
29. Mantegazza, M. A., Bordes, F. & Buzzoni, R. Process for preparing ethyl benzene. US patent 9193643 B2 (2015).
30. Coca-Cola produces world's first PET bottle made entirely from plants. *The Coca-Cola Company* http://www.coca-colacompany.com/press-center/press-releases/coca-cola-produces-worlds-first-pet-bottle-made-entirely-from-plants (2015).
31. Kiricsi, I., Förster, H., Tasi, G. & Nagy, J. B. Generation, characterization, and transformations of unsaturated carbenium ions in zeolites. *Chem. Rev.* **99**, 2085–2114 (1999).
32. Paukshtis, E. A., Malysheva, L. V. & Stepanov, V. G. Interaction of aromatics with Brönsted sites in zeolites: demarcation line between regions of stable existence of H-complexes and ion pairs for various types of bases. *React. Kinet. Catal. Lett.* **65**, 145–152 (1998).
33. Förster, H., Kiricsi, I., Tasi, G. & Hannus, I. Interaction of aromatic compounds with zeolite HZSM-5 studied by UV/VIS spectroscopy. *J. Mol. Struct.* **296**, 61–67 (1993).
34. Chowdhury, A. D. et al. Initial carbon–carbon bond formation during the early stages of the methanol-to-olefin process proven by zeolite-trapped acetate and methyl acetate. *Angew. Chem. Int. Ed.* **55**, 15840–15845 (2016).
35. Van der Borght, K. et al. Insights into the reaction mechanism of ethanol conversion into hydrocarbons on H-ZSM-5. *Angew. Chem. Int. Ed.* **55**, 12817–12821 (2016).
36. Kiricsi, I., Förster, H. & Tasi, G. Formation of carbocations from C_6 compounds in zeolites. *Stud. Surf. Sci. Catal.* **46**, 355–364 (1989).
37. Olah, G. A. General concept and structure of carbocations based on differentiation of trivalent (classical) carbenium ions from three-center bound penta- or tetracoordinated (nonclassical) carbonium ions. Role of carbocations in electrophilic reactions. *J. Am. Chem. Soc.* **94**, 808–820 (1972).
38. Beck, L. W., Xu, T., Nicholas, J. B. & Haw, J. F. Kinetic NMR and density functional study of benzene H/D exchange in zeolites, the most simple aromatic substitution. *J. Am. Chem. Soc.* **117**, 11594–11595 (1995).
39. Wulfers, M. J. & Jentoft, F. C. The role of cyclopentadienium ions in methanol-to-hydrocarbons chemistry. *ACS Catal.* **4**, 3521–3532 (2014).
40. Wang, W., Jiao, J., Jiang, Y., Ray, S. S. & Hunger, M. Formation and decomposition of surface ethoxy species on acidic zeolite Y. *ChemPhysChem* **6**, 1467–1469 (2005).
41. Andronesi, O. C. et al. Determination of membrane protein structure and dynamics by magic-angle-spinning solid-state NMR spectroscopy. *J. Am. Chem. Soc.* **127**, 12965–12974 (2005).
42. Labokha, A. A. et al. Systematic analysis of barrier-forming FG hydrogels from *Xenopus* nuclear pore complexes. *EMBO J.* **32**, 204–218 (2013).
43. Morris, G. A. & Freeman, R. Enhancement of nuclear magnetic resonance signals by polarization transfer. *J. Am. Chem. Soc.* **101**, 760–762 (1979).
44. Pines, A., Gibby, M. G. & Waugh, J. S. Proton-enhanced NMR of dilute spins in solids. *J. Chem. Phys.* **59**, 569–590 (1973).
45. Gordon, C. P. et al. Metathesis activity encoded in the metallacyclobutane carbon-13 NMR chemical shift tensors. *ACS Cent. Sci.* **3**, 759–768 (2017).
46. Kim, S., Robichaud, D. J., Beckham, G. T., Paton, R. S. & Nimlos, M. R. Ethanol dehydration in HZSM-5 studied by density functional theory: evidence for a concerted process. *J. Phys. Chem. A* **119**, 3604–3614 (2015).
47. Kondo, J. N., Yamazaki, H., Osuga, R., Yokoi, T. & Tatsumi, T. Mechanism of decomposition of surface ethoxy species to ethene and acidic OH groups on H-ZSM-5. *J. Phys. Chem. Lett.* **6**, 2243–2246 (2015).
48. Smith, M. B. & March, J. *March's Advanced Organic Chemistry: Reactions, Mechanisms, and Structure* (Wiley-Interscience, John Wiley & Sons, New Jersey, 2007).
49. Corma, A., Sastre, G. & Viruela, P. M. A quantum-chemical study of para/ortho-toluene alkylation by adsorbed methoxy species on zeolites. *J. Mol. Catal. A Chem.* **100**, 75–85 (1995).

50. Jeener, J., Meier, B. H., Bachmann, P. & Ernst, R. R. Investigation of exchange processes by two-dimensional NMR spectroscopy. *J. Chem. Phys.* **71**, 4546–4553 (1979).
51. Weingarth, M., Demco, D. E., Bodenhausen, G. & Tekely, P. Improved magnetization transfer in solid-state NMR with fast magic angle spinning. *Chem. Phys. Lett.* **469**, 342–348 (2009).

Acknowledgements

This project has received funding from the European Union's Horizon 2020 research and innovation programme under the Marie Skłodowska-Curie grant agreement (no. 704544 to A.D.C.), a European Research Council (ERC) Advanced Grant (no. 321140 to B.M.W.) as well as a Veni grant (no. 722.015.003 to G.T.W.) and a Middelgroot programme (no. 700.58.102 to M.B.) from the Netherlands Organization of Scientific Research (NWO). K.H. is supported by uNMR-NL, an NWO-funded National Roadmap Large-Scale Facility of the Netherlands (grant no. 184.032.207).

Author contributions

A.D.C. and B.M.W. conceived the research ideas and directed the overall project. A.D.C. designed and performed the experiments and analysed the data, in particular the bulk characterization, including the operando UV-vis diffuse reflectance spectroscopy measurements. K.H. collected and processed the NMR data. K.H. and M.B. analysed NMR spectroscopy data. G.T.W. prepared all extrudate materials. G.T.W. and S.C. characterized extrudate materials. A.D.C., K.H. and B.M.W. co-wrote the paper. All authors discussed the results and commented on the different versions of the manuscript.

Competing interests

The authors declare no competing financial interests.

Additional information

Supplementary information is available for this paper at https://doi.org/10.1038/s41929-017-0002-4.

Reprints and permissions information is available at www.nature.com/reprints.

Correspondence and requests for materials should be addressed to B.M.W.

Publisher's note: Springer Nature remains neutral with regard to jurisdictional claims in published maps and institutional affiliations.